J|A|C|S
ARTICLES

Published on Web 05/08/2009

Effect of Surface Ligands on Optical and Electronic Spectra of Semiconductor Nanoclusters

Svetlana Kilina,* Sergei Ivanov, and Sergei Tretiak*

Theoretical Division, Center for Nonlinear Studies (CNLS), Chemistry Division, and Center for Integrated Nanotechnologies (CINT), Los Alamos National Laboratory, Los Alamos, New Mexico 87545

Received January 23, 2009; E-mail: skilina@gmail.com; serg@lanl.gov

Abstract: We investigate the impact of ligands on the morphology, electronic structure, and optical response of the $Cd_{33}Se_{33}$ cluster, which overlaps in size with the smallest synthesized CdSe nanocrystal quantum dots (QDs). Our density functional theory calculations demonstrate significant surface reorganization for both the bare cluster and the cluster capped with amine or phosphine oxide model ligands. We observe strong surface−ligand interactions leading to substantial charge redistribution and polarization effects on the surface. These effects result in the development of hybridized states, for which the electronic density is spread over the cluster and the ligands. The loss of one of the passivating ligands leads to either optically dark or bright additional states inside of the band gap, depending on the position of the leaving ligand on the QD surface. However, for fully ligated QDs, neither the ligand-localized nor hybridized molecular orbitals appear as trap states inside or near the band gap of the QD. Instead, being mostly optically dark, dense hybridized states could open new relaxation channels for high-energy photoexcitations. Comparing QDs passivated by different ligands, we also found that hybridized states are denser at the edge of the conduction band of the cluster ligated with phosphine oxide molecules than that with primary amines. Such a different manifestation of ligand binding may potentially lead to faster electron relaxation in QDs passivated by phosphine oxide than by amine ligands.

1. Introduction

Colloidal quantum dots (QDs) are among the most exhaustively investigated semiconductor nanocrystals because of their high luminescence efficiency, size-tunable emission in a wide range of the visible light spectrum, unmatched photostability, and reasonably long photoexcited lifetimes.[1−5] Several possible technological applications of QDs, such as lasing,[6] fluorescent biotagging,[7] quantum computing,[8] and light-emitting diodes,[9] have been outlined in recent years. In addition, time-resolved experiments in these QDs[10,11] demonstrate very high quantum yields for the formation of two or more electron−hole pairs per absorbed single photon, so-called carrier multiplication (CM), which has a potential for substantial improvements in solar-cell efficiency.[4,12] Altogether, QDs are viewed as a promising material for optoelectronic devices of the future. The main roadblock for the success of these applications is precise control over the photoinduced carrier dynamics and emission properties, which mainly depend on the size, composition, and surface chemistry of the nanocrystals.[13,14]

The surface of the colloidal semiconductor nanocrystals is usually terminated with organic ligands. Typically, these are coordinating organic molecules with large HOMO−LUMO gaps, which are used to remove unsaturated valences (dangling bonds) on the surface of the QD, increase solubility, prevent QD−QD interactions, etc. In general, usage of surface ligands leads to a greater synthetic control over the electronic properties of QDs, particularly improving the radiative quantum yield (QY) of nanocrystals. However, the high surface-to-volume ratio of QDs and imperfect surface passivation, which is mainly determined by the type of ligands, lead to impurities and defects. The latter is likely to add the manifold of additional surface states (trap states) to the electronic structure of the QD and, indeed, affect both radiative and nonradiative carrier dynamics. Thus, recent time-resolved experiments have demonstrated that exciton lifetime, rates of Auger recombination, and efficiency of the CM are strongly affected by the type of ligands passivating the QD surface, and those experiments suggest that

(1) Alivisatos, A. P. *Science* **1996**, *271*, 933–937.
(2) Murray, C. B.; Norris, D. J.; Bawendi, M. G. *J. Am. Chem. Soc.* **1993**, *115*, 8706–8715.
(3) Qu, L. H.; Peng, X. G. *J. Am. Chem. Soc.* **2002**, *124*, 2049–2055.
(4) Nozik, A. J. *Annu. Rev. Phys. Chem.* **2001**, *52*, 193.
(5) Scholes, G. D.; Rumbles, G. *Nat. Mater.* **2006**, *5*, 683–696.
(6) Klimov, V. I.; Mikhailvsky, A. A.; Xu, S.; V., M. A.; Hollingsworth, J. A.; Leatherdale, C. A.; Eisler, M.-J.; Bawendi, M. G. *Science* **2000**, *290*, 314–317.
(7) Dahan, M.; Levi, S.; Luccardini, C.; Rostaing, P.; Riveau, B.; Triller, A. *Science* **2003**, *302*, 442–445.
(8) Gorman, J.; Hasko, D. G.; Williams, D. A. *Phys. Rev. Lett.* **2005**, *95*, 090502.
(9) Coe, S.; Woo, W. K.; Bawendi, M.; Bulovic, V. *Nature* **2002**, *420*, 800–803.
(10) Schaller, R. D.; Sykora, M.; Pietryga, J. M.; Klimov, V. I. *Nano Lett.* **2006**, *6*, 424–429.
(11) Klimov, V. I.; Ivanov, S. A.; Nanda, J.; Achermann, M.; Bezel, I.; McGuire, J. A.; Piryatinski, A. *Nature* **2007**, *447*, 441–446.
(12) Schaller, R. D.; Agranovich, V. M.; Klimov, V. I. *Nat. Phys.* **2005**, *1*, 189–194.
(13) Beard, M.; Midgett, A.; Law, M.; Ellingson, R.; Nozik, A. *Nano Lett.* **2009**, *9*, 1217–1222.
(14) Pandey, A.; Guyot-Sionnest, P. *Science* **2008**, *322*, 929–932.

various and contradicting data on CM efficiency reported in recent literature[15] may be a result of uncontrolled differences in QD surface structure and treatment.[13] Yet, significant technological advantages are expected from synthesizing QDs stabilized by appropriate ligands with diverse surface functionalities. The problem of the well-controlled QDs' functionalities calls for more rigorous studies of surface passivation and the role that ligands play in the optoelectronic properties of QDs.

It is experimentally challenging to resolve spectral features originating from QD−ligand interactions, which do not have direct signatures in the conventional spectroscopies. Using ultrafast probes, it has been established experimentally that intraband carrier relaxation dynamics in QDs depends on capping ligands. For example, samples of CdSe QDs coated with different capping molecules exhibit smaller relaxation rates in dots passivated by thiophenol and pyridine, which are assumed to act as hole traps, compared to dots capped by trioctylphosphine oxide (TOPO).[16,6] However, recent results evidence the negligible role of hole traps in overall carrier relaxation in CdSe QDs; instead, "softer" bases, such as thiol and amine derivatives, have a tendency to slow down relaxation, presumably due to the more covalent character of QD−ligand bonds.[17] Radiative response of QDs is also influenced by surface ligands: passivation of CdSe QDs with primary alkylamines notably increases the QY,[18] whereas thiol-treated CdSe QDs are the least fluorescent.[17,19] X-ray photoelectron spectroscopy (XPS) can provide additional information on the surface composition and structure. For example, three distinct layers of the nanocrystal−including QD core, QD surface, and surface−ligand layers−and a fourth capping layer of trioctylphosphine (TOP) were clearly identified in PbSe QDs.[20] Unfortunately, the resolution of this technique is limited, and literature reports are inconclusive: the presence of two distinct species of Cd ions (core and surface ions) in CdSe QDs has been demonstrated in refs 21 and 22 but was not observed in refs 23 and 24. Nevertheless, existing experimental data illustrate the complex structure of nanocrystals, which is beyond a common model of a single core of atoms and a single passivating agent.

Theoretical modeling could provide valuable insight into these issues. Unfortunately, efforts in this direction have been rather limited due to the high computational cost and uncertainty related to the chemical composition and morphology of the nanocrystals. Early theoretical studies of QDs simulated the surface by assuming an infinite potential barrier around the dot.[25] More sophisticated models of capped CdSe QDs have represented the QD core through the bulk atoms using semiempirical tight-binding[26] and pseudopotential[27] approaches, while the passivating molecules have been modeled through either single oxygen atoms or simplified model potentials.[28] Any realistic model, however, has to explicitly describe bonding between the QD and the ligands, which is lacking from the approaches mentioned above. First-principle quantum-chemical methods, such as density functional theory (DFT), are able to provide this information with a reasonable level of accuracy. Unfortunately, DFT is numerically expensive. Therefore, most DFT calculations simulate the core atoms of QDs on the basis of bulk structures, while dangling bonds on the surface are artificially terminated with covalently bonded hydrogen atoms.[29,30] Only a few reports have addressed the specifics of the electronic structure and binding energies of small clusters of CdSe interacting with a single ligand molecule.[31,32]

Here, we report the results of DFT calculations that provide atomistic information on the morphology, electronic structure, and optical response of small CdSe QDs capped by different types and numbers of ligands. We use the $Cd_{33}Se_{33}$ cluster with ~1.3 nm diameter, which represents one of the smallest CdSe nanocrystals that have been experimentally identified with mass spectroscopy.[33] This cluster belongs to the "magic" structure formed by a closed shell of atoms and having an exceptionally high stability.[33,34] Our interest in such small clusters originates not only from the substantial computational efforts of DFT calculations that limit simulations of systems consisting of only a few hundred atoms. More importantly, recent experiments[35,36] have shown that small magic-sized QDs with diameters <2 nm demonstrate controllable size and shape with atomic precision and reproducible optical properties, including efficient blue-light emission.

This paper is organized as follows: our computational approach is briefly outlined in section 2. In section 3 we analyze in detail the results of our numerical simulations on modification of electronic structure of QDs caused by capping ligands. The emerging trends are summarized in section 4.

2. Computational Methodology

Each studied cluster was initially constructed on a wurtzite lattice with bulk Cd−Se bond lengths and then relaxed to its lowest energy configuration (see Figure 1). The geometry optimization procedure was performed using DFT with a plane wave basis set, as

(15) McGuire, J. A.; Joo, J.; Pietryga, J. M.; Schaller, R. D.; Klimov, V. I. *Acc. Chem. Res.* **2008**, *41*, 1810–1819.
(16) Guyot-Sionnest, P.; Shim, M.; Matranga, C.; Hines, M. *Phys. Rev. B* **1999**, *60*, R2181.
(17) Guyot-Sionnest, P.; Wehrenberg, B.; Yu, D. *J. Chem. Phys.* **2005**, *123*, 074709.
(18) Talapin, D.; Rogach, A.; Kornowski, A.; Haase, M.; Weller, H. *Nano Lett.* **2001**, *1*, 207–211.
(19) Liu, I. S.; Lo, H. H.; Chien, C. T.; Lin, Y. Y.; Chen, C. W.; Chen, Y. F.; Su, W. F.; Liou, S. C. *J. Mater. Chem.* **2008**, *18*, 675–682.
(20) Sapra, S.; Nanda, J.; Pietryga, J. M.; Hollingsworth, J. A.; Sarma, D. D. *J. Phys. Chem. B* **2006**, *110*, 15244–15250.
(21) Winkler, U.; Eich, D.; Chen, Z. H.; Fink, R.; Kulkarni, S. K.; Umbach, E. *Phys. Status Solidi A* **1999**, *173*, 253–259.
(22) Winkler, U.; Eich, D.; Chen, Z. H.; Fink, R.; Kulkarni, S. K.; Umbach, E. *Chem. Phys. Lett.* **1999**, *306*, 95–102.
(23) Nanda, J.; Kuruvilla, B. A.; Sarma, D. D. *Phys. Rev. B* **1999**, *59*, 7473–7479.
(24) Borchert, H.; Talapin, D. V.; McGinley, C.; Adam, S.; Lobo, A.; de Castro, A. R. B.; Moller, T.; Weller, H. *J. Chem. Phys.* **2003**, *119*, 1800–1807.
(25) Ekimov, A. I.; Hache, F.; Schanne-Klein, M. C.; Ricard, D.; Flytzanis, C.; Kudryavtsev, I. A.; Yazeva, T. V.; Rodina, A. V.; Efros, A. L. *J. Opt. Soc. Am. B* **1993**, *10*, 100.
(26) Pokrant, S.; Whaley, K. B. *Eur. Phys. J. D* **1999**, *6*, 255–267.
(27) Wang, L. W.; Zunger, A. *Phys. Rev. B* **1996**, *53*, 9579–9582.
(28) Reboredo, F. A.; Zunger, A. *Phys. Rev. B* **2001**, *63*, 235314–235317.
(29) Dalpian, G. M.; Tiago, M. L.; del Puerto, M. L.; Chelikowsky, J. R. *Nano Lett.* **2006**, *6*, 501–504.
(30) del Puerto, M. L.; Tiago, M. L.; Chelikowsky, J. R. *Phys. Rev. Lett.* **2006**, *97*, 096401–096404.
(31) Puzder, A.; Williamson, A.; Zaitseva, N.; Galli, G.; Manna, L.; Alivisatos, A. *Nano Lett.* **2004**, *4*, 2361–2365.
(32) Rempel, J. Y.; Trout, B. L.; Bawendi, M. G.; Jensen, K. F. *J. Phys. Chem. B* **2006**, *110*, 18007–18016.
(33) Kasuya, A.; et al. *Nat. Mater.* **2004**, *3*, 99–102.
(34) Pedersen, J.; Bjornholm, S.; Borggreen, J.; Hansen, K.; Martin, T. P.; Rasmussen, H. D. *Nature* **1991**, *353*, 733–735.
(35) Evans, C. M.; Guo, L.; Peterson, J. J.; Maccagnano-Zacher, S.; Krauss, T. D. *Nano Lett.* **2008**, *8*, 2896–2899.
(36) Kudera, S.; Zanella, M.; Giannini, C.; Rizzo, A.; Li, Y.; Gigli, G.; Cingolani, R.; Ciccarella, G.; Spahl, W.; Parak, W. J.; Manna, L. *Adv. Mater.* **2007**, *19*, 548–552.

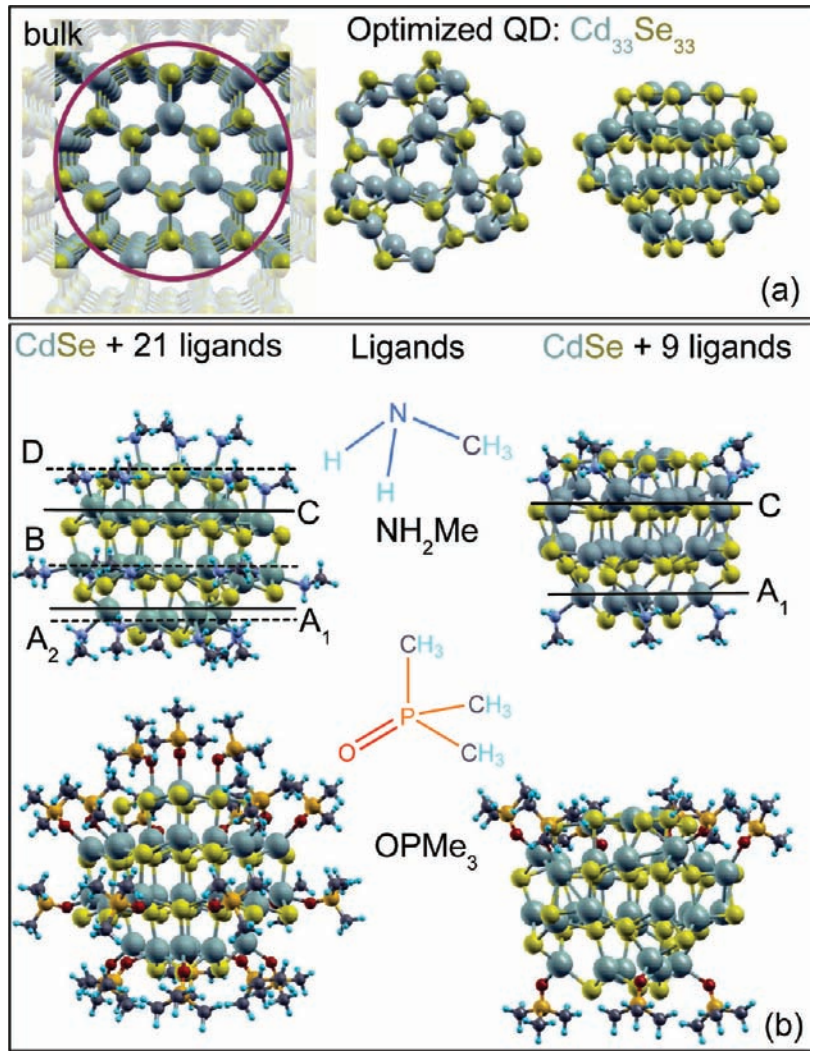

Figure 1. Structures of the studied CdSe QDs. (a) Schematic representation of the QD construction from the ideal CdSe bulk (left) and the optimized geometry of the $Cd_{33}Se_{33}$ showing (0001) (middle) and $(01\bar{1}0)$, $(11\bar{2}0)$ facets (right) calculated using GGA (VASP) methodology. (b) The GGA optimized geometries of passivated $Cd_{33}Se_{33}$ (right and left columns). The middle column shows chemical structures of considered ligands—methylamine (NH_2Me) and trimethylphosphine oxide ($OPMe_3$)—used as models for primary amines and trioctylphosphine oxide (TOPO), respectively. Nine ligands are attached only to two-coordinated Cd atoms marked as A_1 and C; 21 ligands are attached to both two-coordinated (A_1 and C) and three-coordinated (A_2, B, and D) Cd atoms.

incorporated to the VASP code.[37] The generalized gradient approximation (GGA) functional of Perdew and Wang (PW91)[38] coupled with the Vanderbilt pseudopotentials[39] was used in order to account for the electron exchange and correlation effects. The simulations were carried out in a cubic cell periodically replicated in three dimensions, as stipulated by the plane wave basis. To prevent spurious interactions between periodic images of the QD, the cell is constructed to have at least 8 Å of vacuum between the QD replicas. As this procedure relaxes the structure into a local energy minimum, we repeated the relaxation from a variety of starting points, with and without surface passivation. Each time, we found nearly identical final structures, with subtle changes corresponding to total energy differences significantly smaller than room temperature. The majority of such conformational configurations has very similar electronic structure, with variation in the values of the energy gap being less than 0.001 eV. Additionally, we optimized geometries using local density approximation (LDA) and Hartree−Fock (HF) with localized Gaussian basis sets LANL2dz using the Gaussian 03 software package.[40] As expected, we found that the ground-state potential energy surface is fairly flat with respect to the steric conformations of surface agents.

It is well established that electronic structure calculations based on the GGA or LDA functional severely underestimate energy gaps (see Supporting Information, Figure S1) and long-range nonlocal Coulombic interactions.[29−32,41] Hybrid functionals such as B3LYP include a portion of the exact HF exchange and are routinely used to partially remedy the above problem, providing values of the calculated gaps very close to experimental data.[42] Therefore, using optimal geometries, we finally calculate the electronic structure and the optical response of QDs with the hybrid B3LYP functional incorporated into Gaussian 03 code. The LANL2dz basis set is used for all Gaussian calculations. Our previous study has shown that

(37) Kresse, G.; Furthmüller, J. *Phys. Rev. B* **1996**, *54*, 11169.
(38) Perdew, J. P. *Electronic Structure of Solids*; Ziesche, P., Eschrig, H., Eds.;Akademie Verlag: Berlin, 1991.
(39) Vanderbilt, D. *Phys. Rev. B* **1990**, *41*, 7892.
(40) Frisch, M. J.; et al. *Gaussian 03*, Revision D.02; Gaussian, Inc.: Wallingford, CT, 2004.
(41) Puzder, A.; Williamson, A. J.; Gygi, F.; Galli, G. *Phys. Rev. Lett.* **2004**, *92*, 217401.
(42) Tretiak, S.; Igumenshchev, K.; Chernyak, V. *Phys. Rev. B* **2005**, *71*, 33201.

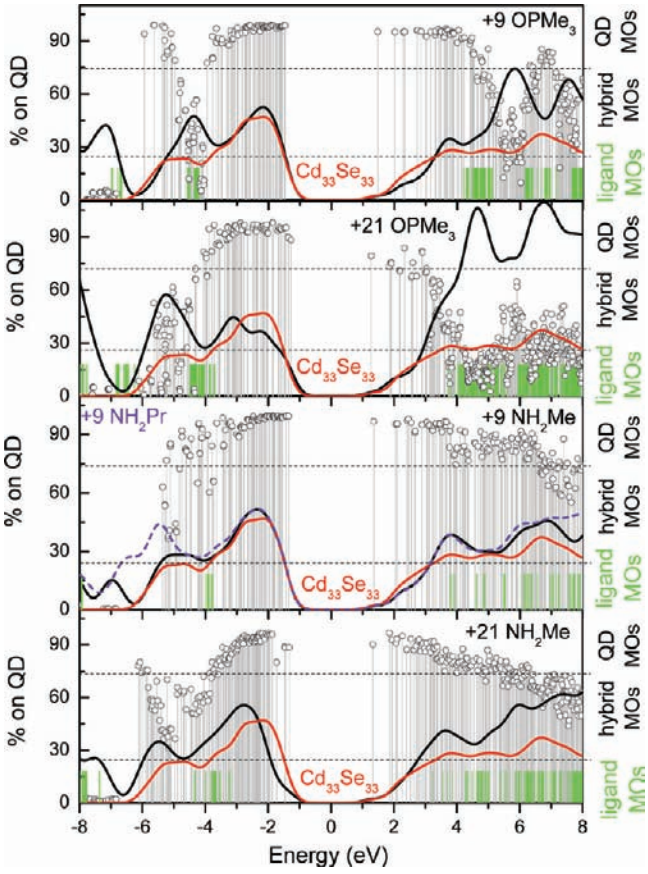

Figure 2. Density of states (DOS) and percent of the Kohn−Sham wave function localization (α_k, see eq 3) on the QD for the $Cd_{33}Se_{33}$ cluster calculated using the B3LYP/LANL2dz method. The red line shows the DOS of the bare QD, and the black line shows the DOS of the QD ligated by 9 and 21 molecules of $OPMe_3$ (a,b) or NH_2Me (c,d). The dashed violet line corresponds to the DOS of $Cd_{33}Se_{33}$ ligated by 9 molecules of $CH_3(CH_2)_2NH_2(NH_2Pr)$. The Fermi energy is chosen to be in the middle of the HOMO−LUMO gap, and Gaussian broadening of 0.2 eV is used for the DOS calculations. Vertical gray lines correspond to the energies of electronic states, and their length shows the percent of the wave function that is localized on the QD. Orbitals with $\alpha_k \gtrsim 75\%$ and $\alpha_k \lesssim 25\%$ are considered to be the QD and ligand MOs, respectively. Delocalized states with $25\% \lesssim \alpha_k \lesssim 75\%$ are defined as *hybridized* MOs, which have charge density on both QD and ligand atoms. Green lines show the pure ligand MO energies, when the Cd/Se atoms are removed from the optimized ligated QDs.

such theoretical methodologies describe well a minimal CdSe cluster bound to the most common ligands.[43]

The density of states (DOS) and optical absorption spectra of QDs are calculated within the single-particle Kohn−Sham orbital representation using Gaussian line-broadening:

$$A(\omega) = \frac{1}{\sigma\sqrt{\pi}} \sum_n h_n \exp\frac{-(\omega_n - \omega)^2}{\sigma^2} \qquad (1)$$

where ω_n and h_n are the energy and the strength of the transition and σ is the width of the spectral peak. These quantities are as follow: for DOS calculations in Figures 2 and 3, $\omega_n = \varepsilon_k$ and $h_n = 1$ (ε_k being the energy of molecular orbitals (MOs)); for density of transitions (DOT) shown in Figure 6, $\omega_n = \varepsilon_k - \varepsilon_l$ and $h_n = 1$ (ε_k and ε_l being the energies of virtual and occupied MOs, respectively); for optical spectra in Figures 3−6, $\omega_n = \varepsilon_k - \varepsilon_l$ and $h_n = f_{kl}$ (f_{kl} being the oscillator strength of the transition). The oscillator strength, f_{kl}, of each transition is defined as

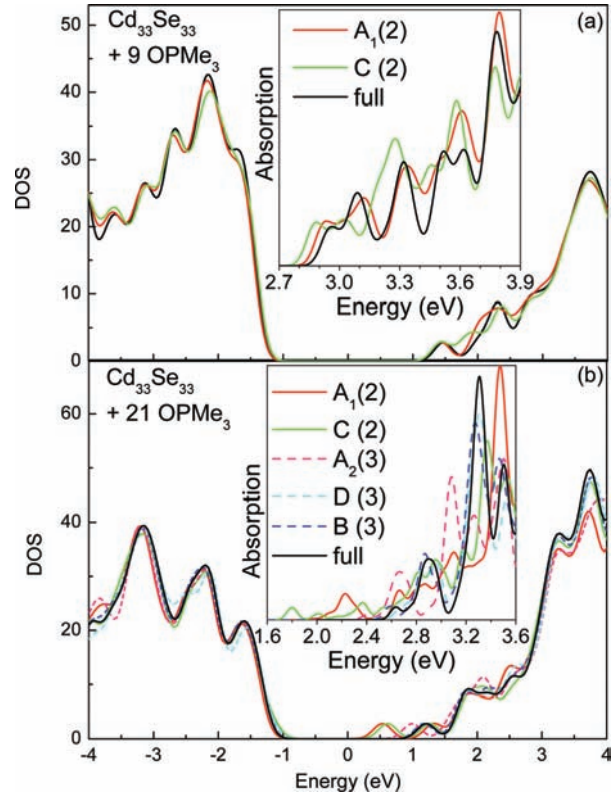

Figure 3. Electronic and optical spectra of the $Cd_{33}Se_{33}$ ligated by $OPMe_3$ molecules when one of the ligands is removed from the optimized structure. The line-broadening parameters $\sigma = 0.1$ eV and $\sigma = 30$ meV are used to calculate DOS and absorption spectra (insets), respectively. The spectra of QDs fully ligated by either 9 (a) or 21 (b) ligands are shown in solid black. The solid green and red lines correspond to the spectra of the ligated QD with one $OPMe_3$ removed from the two-coordinated Cd atom of the type A_1 or C, respectively. The dashed lines show the spectra of the ligated QD with one ligand removed from the three-coordinated Cd atom of the type A_2, B, or D.

$$f_{kl} = \frac{2m_e(\varepsilon_k - \varepsilon_l)}{3\hbar^2}\mu_{kl}^2 \qquad (2)$$

where μ_{kl} is the transition dipole moment (see eq 4). Chosen line-width parameters σ are indicated in the figure captions. For example, for calculation of optical spectra, we chose $\sigma = 30$ meV, which is comparable with experimental inhomogeneous broadening due to size distribution effects. DOS spectra are simulated using $\sigma = 100$ meV.

Such single-particle mean-field representation can be used as a zeroth-oder approximation for calculation of absorption spectra of semiconductor QDs, since its optical properties are dominated by quantum confinement effect (the Coulomb energy for small QDs is much smaller than the kinetic energy and can be treated as a first-order perturbation[25]). More advanced approaches incorporating many-body correlation effects including Coulombic interactions between photoexcited electrons and holes, such as the Bethe−Salpeter theory and time-dependent density functional theory (TDDFT),[30,44] can produce better agreement with the experimental data. Unfortunately, they are computationally demanding and cannot be applied yet to systems of the considered sizes. To check the effect of electron−hole correlations on the optical response of the CdSe QDs,

(43) Yang, P.; Tretiak, S.; Masunov, A.; Ivanov, S. *J. Chem. Phys.* **2008**, *129*, 074709.

(44) Onida, G.; Reining, L.; Rubio, A. *Rev. Mod. Phys.* **2002**, *74*, 601–659.

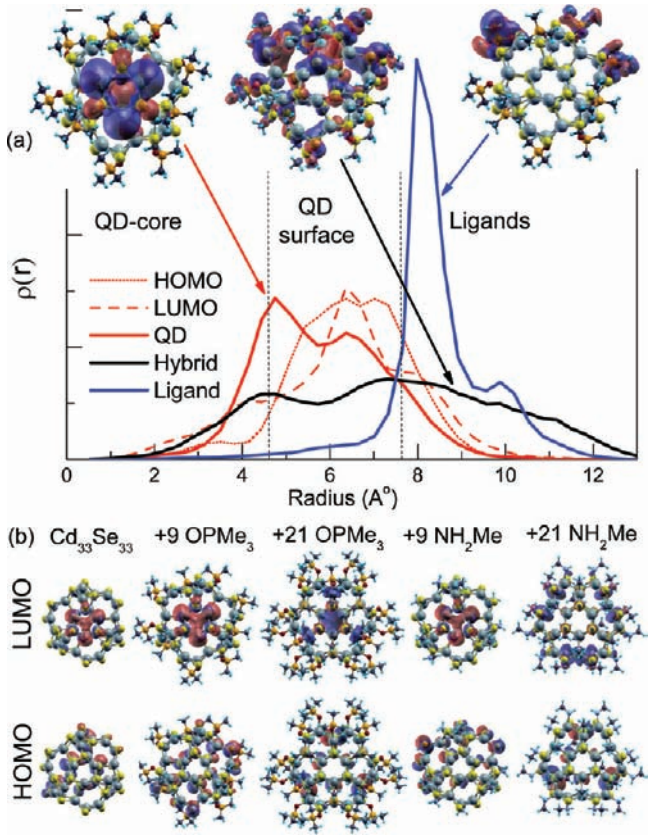

Figure 4. (a) Molecular orbitals representing typical states localized on the QD, localized on ligands, and delocalized over the QD and ligands (hybridized MOs), and their corresponding angle-averaged electronic density distributions $\rho(r)$ calculated as functions of the QD radius of $Cd_{33}Se_{33}$ ligated by 9 molecules of $OPMe_3$. The vertical dashed lines indicate the QD interior, including all four-coordinated Cd and Se atoms (the core) and the border between the QD surface and ligands. (b) Plots of HOMO and LUMO for the bare and ligated QDs. The (0001) facet of all QDs is oriented toward the viewer. For all QDs, both HOMO and LUMO are surface states: HOMO is mostly distributed over Se atoms on the $(000\bar{1})$ facet, while LUMO is spread over Cd and Se atoms on the (0001) facet. For full capping with 21 ligands, when all surface Cd atoms are passivated, the LUMO is significantly changed from the LUMO of the bare and partially passivated QDs, showing that ligands do affect surface states.

we calculate absorption spectra of the uncapped CdSe cluster and the isolated ligand molecules using two methods: many-body TDDFT and the single-particle Kohn−Sham approach (see Supporting Information, Figure S6). As can be seen from Figure S6, the single-particle spectrum of the $Cd_{33}Se_{33}$ is blue-shifted by ∼0.34 eV compared to the spectrum obtained from TDDFT calculations. The overall line shape of the uncorrelated spectrum roughly follows the shape of the correlated spectrum. This result establishes approximate margins of error in our single-particle Kohn−Sham orbital approach to the spectra of the QDs we study. Notably, the electronic correlations shift to the red by 1−1.5 eV and significantly change the spectra of isolated ligands, demonstrating the importance of many-body correlations for ligands.

3. Results and Discussion

3.1. Description of Considered Clusters. It is well established that experimentally studied QDs retain in the core the original crystal structure. Figure 1a schematically shows our construction of $Cd_{33}Se_{33}$ from a wurtzite lattice with bulk Cd−Se bond lengths. The analogous construction of CdSe clusters from the bulk semiconductor has been used in previous theoretical studies.[31,41,45] In addition to the uncapped ("bare") $Cd_{33}Se_{33}$, we also simulate clusters with 9 and 21 ligands attached to the surface of the dot. Chosen capping groups—trimethylphosphine oxide ($OPMe_3$) and methylamine (NH_2Me)—are reduced models that chemically well represent[31,43] TOPO and primary amines commonly used as passivating ligands for CdSe QDs.

Our previous studies[43] and Rempel et al.[32] have shown computationally that the dominant binding interactions occur between O or N atoms of the ligand and Cd atoms on the QD surface. The results of XPS experiments[19] also prove that ligands such as TOPO, thiophenol, toluenethiol, and *p*-hydroxythiophenol bind much more strongly to the Cd atoms than to the Se atoms of the QDs. In $Cd_{33}Se_{33}$, two types of Cd atoms can interact with ligands: two-coordinated Cd atoms that are bonded to only two Se atoms, having two unsaturated valences (marked as A_1 and C in Figure 1), and three-coordinated Cd atoms that are bound to three Se atoms, having one unsaturated valence (marked as A_2, B, and D in Figure 1). Note that one-coordinated Cd atoms having three unsaturated valences are chemically unstable toward dissociations and cannot be part of the QD surface. To simulate the Cd−ligand interaction, we initially place 9 molecules of either $OPMe_3$ or NH_2Me near all two-coordinated Cd atoms. Such Cd atoms are speculated to be more chemically active than three-coordinated ones because of the higher number of unsaturated valences. Therefore, we assume that ligand binding most likely starts with the saturation of nine surface Cd atoms with the maximum number of dangling bonds. To saturate the rest of the surface Cd atoms, 12 additional capping ligands were attached, resulting in the full passivation of the $Cd_{33}Se_{33}$ cluster by 21 molecules. Thus, our simulations allow us to study the difference between ligand binding to two- and three-coordinated Cd atoms and the effects of these differences on the electronic structure and optical response of the ligated CdSe QD.

3.2. Geometry Structures and Bonding. As can be seen in Figure 1, the final geometries of all clusters deviate from the initial bulk configuration, although the rough bulk-like structure is still recognizable. The Cd−Se bonds in the center of the QD are about 4% longer compared to the experimental values of Cd−Se bonds in the bulk material. Our previous VASP calculations[45] of the wurtzite structure of the CdSe bulk provide Cd−Se bonds of ∼2.67 Å, which are ∼2% smaller compared to analogous calculations of Cd−Se bonds in the core of the $Cd_{33}Se_{33}$ cluster. Although optimization leads to an increase of the bond length between inner atoms of the QD compared to the bulk, the optimized bonds between Cd and Se atoms on the surface are 2−3% shorter than those in the QD core. This is indicative of the surface reconstruction that results in closer positioning of Se and Cd atoms on the surface, even in the presence of passivating ligands. Due to the surface reconstruction, all surface Cd atoms become three-coordinated in the bare QD. When 9 capping molecules are optimized on the QD surface, all surface Cd atoms become either three- or four-coordinated. In the case of the full passivation by 21 ligands, all Cd atoms on the surface become four-coordinated when optimization is completed.

Table 1 compares the average bond lengths in the optimized QDs for surface Cd atoms having three neighboring Se atoms (Cd−Se(3)) and for interior four-coordinated Cd atoms having four neighboring Se atoms (Cd−Se(4)), as well as bonds between atoms in the ligands adsorbed onto the QD surface. Bond lengths obtained from the geometry optimizations with

(45) Kamisaka, H.; Kilina, S. V.; Y, Y.; Prezhdo, O. V. *J. Phys. Chem. C* **2008**, *112*, 7800–7808.

Table 1. Bond Lengths (Å) and Band Gaps (eV) in the Bare and Capped CdSe QDs, Whose Geometries Are Optimized by Different Functionals with LANL2dz Basis Set

system	bonds	GGA	LDA	HF
bare	Cd−Se(3)	2.64	2.69	2.67
$Cd_{33}Se_{33}$	Cd−Se(4)	2.73	2.76	2.79
	band gap[a]	2.80	2.71	2.48
$Cd_{33}Se_{33}$	Cd−Se(3)	2.65	2.71	2.70
+ 9 $OPMe_3$	Cd−Se(4)	2.71	2.74	2.77
	Cd−O	2.34	2.17	2.17
	O═P	1.51	1.65	1.61
	P−C	1.81	1.85	1.84
	band gap[a]	2.94	2.85	2.82
$Cd_{33}Se_{33}$	Cd−Se(3)	2.67	2.71	2.73
+ 21 $OPMe_3$	Cd−Se(4)	2.73	2.73	2.78
	Cd−O	2.40	2.19	2.22
	O═P	1.50	1.64	1.61
	P−C	1.81	1.85	1.84
	band gap[a]	2.60	2.67	2.48
$Cd_{33}Se_{33}$	Cd−Se(3)	2.65	2.70	2.69
+ 9 NH_2Me	Cd−Se(4)	2.72	2.75	2.78
	Cd−N	2.44	2.31	2.36
	N−C	1.48	1.48	1.49
	band gap[a]	2.99	2.87	2.70
$Cd_{33}Se_{33}$	Cd−Se(3)	2.67	2.73	2.71
+ 21 NH_2Me	Cd−Se(4)	2.72	2.77	2.79
	Cd−N	2.44	2.32	2.39
	N−C	1.47	1.47	1.48
	band gap[a]	2.66	2.68	2.65

[a] Band gaps are calculated with the B3LYP/LANL2dz method using geometries obtained from GGA, LDA, and HF optimizations.

different functionals are also presented in this table. In general, both LDA and HF simulations provide longer Cd−Se bonds compared to the GGA results, while the Cd−ligand bonds are longer for GGA calculations. Nonetheless, all methods predict similar trends in bond lengths of the QD: surface Cd and Se atoms, e.g., atoms bound to three neighboring atoms, have shorter bonds than those bound to four neighbors in the interior of the QD. Shorter distances also result in decreasing the Cd−Cd and Se−Se separation on the surface. For instance, in both bare and capped QDs, the distance between the two closest Se atoms on the surface is ∼3.9 Å, compared to ∼4.5 Å between the nearest Se in the center of the QDs. For the nearest Cd atoms, the distance is ∼3.7 Å when they are on the surface and ∼4.5 Å when they are in the center of the QD. The decrease in Se−Se separation may facilitate formation of Se−Se bridges on the surface of QDs.[33,43] In addition, the difference between the Cd−Se bonds in the core and on the surface of the clusters points to the significant deviation of the surface morphology from that of the QD interior. While our results are based on the small CdSe clusters, the QD−core, QD−surface, and ligand−surface layers were experimentally detected in CdS, CdSe,[21,22] and PbSe[20] nanocrystals, thus supporting our conclusion for the general case of the larger QDs.

3.3. Surface Reconstruction, Gap Opening, and Trap States. The trend of decreasing bond lengths and Cd−Cd/Se−Se separations on the surface is much alike in both bare and passivated QDs; i.e., significant surface reconstruction occurs even in the presence of ligands passivating the QD's surface. Surface reconstruction results in the saturation of dangling bonds (self-healing), so that two- and three-coordinated Cd atoms become three- and four-coordinated, respectively. Such a bond saturation leads to removal of surface states from inside of the band gap of all clusters we considered (see Figure 2 and Supporting Information, Figure S1). Previous DFT calculations[41] of the electronic structure of the bare $Cd_{15}Se_{15}$ and $Cd_{33}Se_{33}$ clusters have also evidenced that geometry optimization leads to the surface reconstruction that saturates dangling bonds and opens the simulated HOMO−LUMO gap. However, surface reconstructions are supposed to be more effective in small clusters compared to large nanocrystals. Based on its bulk lattice structure, any QD can be represented as a convex polyhedron. Atoms of the QD thus are attributed to vertices, edges, faces, and inner body (the core) of this polyhedron. The number of edge, face, and body atoms in QD grows as a function of R, R^2, and R^3, respectively, with QD radius R. As such, the fraction of low-coordinated edge and face atoms is the largest for small QDs. Core atoms are fully coordinated and preserve nearly bulk structure. Face atoms typically lack one neighbor, while edge atoms lack two neighbors. Vertex atoms may lack three neighbors. The atoms lacking a larger amount of neighbors experience the most substantial reconstruction. Thus, the relative number of atoms that are subject to substantial reconstruction rises with decreasing QD size, leading to more effective surface reconstructions and band gap opening in small clusters.

Figure 2 shows the DOS calculated using eq 1 for the bare and capped $Cd_{33}Se_{33}$ QDs. All QDs demonstrate a well-pronounced energy gap of ∼3 eV, which fortuitously agrees well with the lowest absorption peak (∼2.99 eV) experimentally observed and assigned to the $Cd_{33}Se_{33}$ QD.[33,36] The comparison of band gap values in the bare and capped clusters calculated with B3LYP and different optimized geometries is presented in Table 1. The optimized bare cluster has a well-opened band gap; moreover, this gap is slightly larger compared to that of the $Cd_{33}Se_{33}$ cluster passivated by 21 ligands. Such fluctuations in energy gaps are likely to originate from polarization effects on the surface of the QD, which depend on the type and the number of passivating ligands and directions and absolute values of their static dipoles.

In fact, not every ligand on the surface interacts identically with the QD. This interaction originates from a specific geometrical position of each ligand on the QD surface and on ligand binding to either two- (A_1 and C) or three-coordinated (A_2, B, and D, Figure 1) Cd atoms. Table 2 shows the binding energies of each of the ligand types calculated as the difference between total energies of the QD passivated by the full amount of ligands (either 9 or 21), the QD lacking one of the ligands, and an isolated optimized ligand. An extended version of this table is shown in the Supporting Information (Table S1). As expected, ligands connected to the two-coordinated Cd atoms, (C in Figure 1b) typically have the largest binding energy, especially in the case of $OPMe_3$ ligation. The average binding energy is slightly higher for the cluster fully passivated with $OPMe_3$ ligands. However, $OPMe_3$ ligands connected to three-coordinated Cd atoms (B and D) experience weaker interactions compared to analogous NH_2Me ligands. The small binding energies of some $OPMe_3$ ligands can be explained by stronger steric interactions of $OPMe_3$ molecules, compared to the smaller in size NH_2Me ligands.

To analyze modification of the electronic structure introduced by a loss of the ligand, we remove one ligand molecule of each type from the optimized ligated QD and calculate the DOS and absorption spectra of the "reduced" system. The absence of one of the 9 $OPMe_3$ ligands that is connected to two-coordinated Cd atoms insignificantly changes the DOS and absorption spectra (see eq 1), as shown in Figure 3. The lack of one of

those ligands does not introduce any trap states into the energy gap. This is because surface reconstruction in these QDs is very similar to that of the bare QD: surface Cd atoms that are initially bound to two Se atoms become bound to three Se atoms after optimization. Thus, all Cd atoms on the surface stay either four- or three-coordinated, even if one of the ligand molecules is lost. However, each of these 9 molecules is bound very strongly to the QD surface, so that a ligand can be hardly lost due to thermal fluctuations (see Table 2). For the QD ligated by 21 ligands, no trap states are introduced to the energy gap and no noticeable change in the absorption spectra is seen when one weakly interacting ligand of the A, B, and D types is lost from the three-coordinated Cd atoms (see Table 2). In contrast, the QD lacking the strongly interacting A_1 or C ligand from 21 capping molecules is revealed by an appearance of the trap states inside of its band gap, as shown in Figure 3b. Such trap states originate from unoccupied molecular orbitals, which are strongly localized on the Cd atoms that have lost the ligand and on two neighboring surface Se atoms. Analogous results are obtained for amine-passivated QDs (see Supporting Information, Figure S5).

Noteworthy, the removal of the $OPMe_3$ ligand of the C type leads to trap states that are weakly allowed optically, resulting in small, low-energy peaks in the absorption spectra, while the lowest energy trap states originating from the A_1 type of $OPMe_3$ ligands are optically dark (see Figure 3b). Consequently, losing the strongly interacting ligands of the fully ligated QDs can significantly affect the optical spectra, leading to the appearance of either dark or semibright trap states inside of the band gap of the QD. Ligands attached to the three-coordinated Cd atoms interact weakly with the QD surface and can be easily lost due to thermal fluctuations, while not significantly affecting optical and electronic response of ligated CdSe QDs. The presence of the dark and bright trap states is in agreement with experimental findings revealed during the synthesis of CdSe QDs. It has been known that some batches of CdSe nanocrystals exhibit only low-efficiency band-edge emission (manifestation of dark trap states present), whereas other batches of CdSe QDs might also reveal the second emission band of semibright trap states around 600−700 nm. Such trap states may be strongly involved in photoinduced charge dynamics in the nanocrystals (e.g., refs 6, 15, 17, 18).

3.4. Electronic Structure of Valence and Conduction Bands. The DOS of the bare and ligated clusters is roughly the same near the edge of the energy gap (see Figure 2). However, inside the bands, the DOS of the capped clusters reveals a lot of additional states resulting in new intense peaks in the DOS of the passivated clusters compared to the bare QD. To analyze the spatial extent of the underlying wave functions and their localization on QD and ligand atoms, we further expand molecular orbitals (MOs) $\{\psi_k\}$ in terms of the respective atomic orbital (AO) basis $\{\chi_i\}$ as

$$\psi_k = \sum_i a_{ik}\chi_i^{QD} + \sum_j b_{jk}\chi_j^{LG} \quad (3)$$

The coefficients $\alpha_k = 100\sum_i a_{ik}^2$ and $\beta_k = 100\sum_b b_{jk}^2$ are fractions of the kth orbital density on the QD and ligands, respectively ($\alpha_k + \beta_k = 100\%$). Gray vertical lines in Figure 2 show the α_k distribution for ligated clusters. In the energy regions where the DOS of the bare QD significantly deviates from the DOS of the capped clusters, most of the states have α_k varying between 25% and 75%. Consequently, most of these "extra" states are spread over both QD and ligand atoms; therefore, we refer to these molecular orbitals as the *hybridized states*. States near the band gap have wave functions mostly localized on the QD atoms ($\alpha_k \gtrsim 75\%$), explaining why the DOS of the bare and capped QDs nearly coincide in this region. Pure ligand states ($\alpha_k \lesssim 25\%$) mostly appear deep inside the VB.

Thus, all capped QDs have three types of molecular orbitals: MOs localized on the QD, MOs localized on ligands, and hybridized orbitals (see Figure 2). For illustration, three-dimensional representations of a few MOs belonging to each of these types are shown in Figure 4. This figure also shows the angle-averaged electronic density distributions of these MOs as a function of the radius of the QD in spherical coordinates, $\rho_k(r) = \int_\varphi \int_\Theta |\psi_k(r,\varphi,\Theta)|^2 \, d\varphi \, d\Theta$. The border between the core and the surface of the QD, shown as a vertical dashed line in Figure 4a, is determined as the average maximum radius (r) from the QD center of mass to the interior four-coordinated Cd and Se atoms. The border between the QD surface and ligands is found as follows: The radius is averaged over r of the most distant Cd and Se atoms from the center of the mass of the QD, and then half of the averaged Cd−O (Cd−N) bond length is added. Such definition is not precise, and usage of eq 3 for quantification of MO localization is preferential. As expected, $\rho(r)$ of the hybridized states has two pronounced peaks showing localization of the charge density on the QD, as well as on the ligand atoms. As can be seen in Figure 4b, the HOMO and LUMO of all passivated clusters are localized on the surface Cd and Se atoms and do not originate from the ligands. Interestingly, HOMO and LUMO look similar for the bare QD and the QD capped by 9 molecules of either $OPMe_3$ or NH_2Me, while they are more distinct for the cluster passivated by 21 ligands. This difference shows that the ligand passivation can, indeed, affect the surface states of the QD, leading to slight changes in values of the energy gaps of QDs passivated by different number/types of ligands.

Let us analyze ligand-localized orbitals in the passivated QDs and, specifically, focus on differences between NH_2Me and $OPMe_3$ capping. As can be seen from Figure 2, the energies of ligand-localized MOs roughly coincide with energies of interacting ligands when the $Cd_{33}Se_{33}$ part is removed from the ligated QD (green lines in Figure 2). For the QDs capped by 21 molecules (when ligands are much closer to each other,

Table 2. Ligand−QD Bond Lengths (Å) and Average Binding Energy Per Ligand Molecule (eV/Ligand) in the Capped CdSe QDs[a]

Cd atoms		$Cd_{33}Se_{33} + n\ OPMe_3$				$Cd_{33}Se_{33} + n\ NH_2Me$			
		$n = 9$		$n = 21$		$n = 9$		$n = 21$	
type	number	Cd−O	E_{bind}	Cd−O	E_{bind}	Cd−N	E_{bind}	Cd−N	E_{bind}
A_1 (2-coord)	3	2.39	−0.61	2.30	−0.76	2.45	−0.71	2.49	−0.98
A_2 (3-coord)	3			2.36	−0.73			2.39	−0.47
B (3-coord)	6			2.39	−0.46			2.50	−0.48
C (2-coord)	6	2.33	−0.66	2.34	−1.37	2.42	−0.69	2.36	−0.95
D (3-coord)	3			2.49	−0.23			2.51	−0.40
average		2.35	−0.64	2.38	−0.77	2.43	−0.69	2.44	−0.67

[a] Binding energies are calculated using VASP code, PW91 functional, and plane wave basis set.

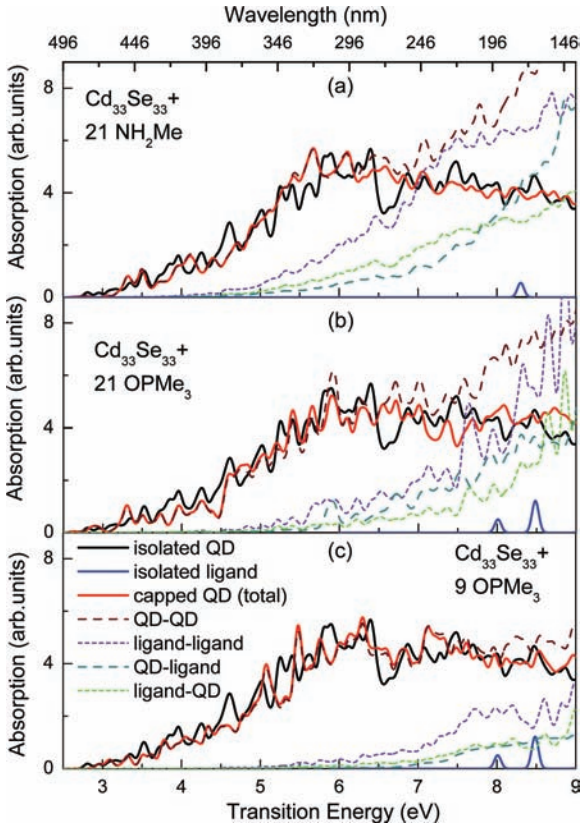

Figure 5. Absorption spectra of $Cd_{33}Se_{33}$ calculated with and without ligands using line-broadening parameter $\sigma = 30$ meV. The black line corresponds to the bare $Cd_{33}Se_{33}$, and the blue line shows the isolated ligand molecules of NH_2Me (a) and $OPMe_3$ (b,c). The red line represents the optical spectra of the $Cd_{33}Se_{33}$ capped by 21 molecules of NH_2Me (a), 21 molecules of $OPMe_3$ (b), and 9 molecules of $OPMe_3$ (c). Dashed lines show optically allowed transitions between valence and conduction bands calculated according to eq 4, decomposing the optical spectrum into four distinct contributions: QD−QD, ligand−ligand, QD−ligand, and ligand−QD. Low-energy transitions are nearly completely defined by QD states, while high-energy excitations may generate transitions between hybridized states or ligand states.

compared to the QDs passivated by 9 ligands), strong ligand−ligand interactions shift ligand states closer to the band gap of the QD for both NH_2Me- and $OPMe_3$-ligated QDs. These shifts are attributed to ligand−ligand interactions on the following basis: When ligands are well separated spatially (noninteracting case), the absorption spectra of 9 molecules and 21 molecules nearly coincide (see Supporting Information, Figure S2). Surprisingly, there are almost no MOs completely localized on ligands in the CB of the QD passivated by NH_2Me. Pure ligand states appear only inside of the VB sub-band gap, where no QD's states contribute to the DOS of the bare cluster. In contrast, the QDs ligated by $OPMe_3$ molecules have a considerable amount of pure ligand states not only in their VB but also in the CB. However, some of this increase in the orbital localization on the $OPMe_3$ might be attributed to an incomplete basis set size. As expected, increasing the basis set for the ligand atoms uniformly enhances the delocalization of orbitals, while qualitatively the structure of the electronic state delocalization stays the same (see Supporting Information, Figure S3). Particularly, for B3LYP calculations with the combined basis set of LANL2dz for QD atoms and 6-31G* for ligand atoms, we do not observe pure ligand-localized states in the CB: all MOs have $\alpha_k > 25\%$ for clusters passivated by either $OPMe_3$ or NH_2Me ligands. However, strongly localized ligand states are seen in the VB (at ∼−4.5 eV) of the QD ligated by $OPMe_3$. Such states are not present in the DOS of the QD passivated by NH_2Me, except the regions of sub-band gaps in the VB (at ∼−7 eV). An extension of the basis set does not change the overall qualitative picture of MO delocalization. Therefore, we conclude that QDs ligated by $OPMe_3$ have more states strongly localized on the QD (trap states) than QDs ligated by NH_2Me molecules.

For both passivating agents, however, hybridized states dominate. Strong QD−ligand interaction results in substantial hybridization of ligand and QD orbitals. The calculated binding energies presented in Table 2 clearly indicate a strong binding between the QD and ligands. Yet, weaker binding of the QD to some $OPMe_3$ molecules, compared to NH_2Me molecules, especially when a ligand interacts with the three-coordinated Cd atoms, can explain the more localized character of ligand MOs in the QD ligated by $OPMe_3$. Also the more localized character of O−P bond and, in particular, the mainly nonbonding lone pair on oxygen in the $OPMe_3$, compared to N−C bond in the NH_2Me molecules, might be an additional origin of stronger localization of ligand MOs in the $OPMe_3$-ligated QDs.

An additional important feature of $OPMe_3$ capping is very dense ligand sub-bands of unoccupied orbitals (green lines in Figure 2), resulting in the high peaks in the CB of the ligated cluster. In contrast to amine-passivated QDs, the density of ligand and hybridized states is considerably larger inside the CB compared to the VB in the cluster passivated by phosphine oxide ligands, particularly in the case when 21 $OPMe_3$ molecules are bound to the surface. This difference does not originate from the difference between $OPMe_3$ and NH_2Me sizes. Substitution of NH_2Me molecules with propylamine ($NH_2CH_2CH_2CH_3$), comparable in the number of atoms with $OPMe_3$, does not significantly change the DOS within the energy interval of $E_{gap} \pm 4$ eV (the dashed line in Figure 2 and Supporting Information, Figure S4). Because of denser CB with a dominant contribution from the hybridized states, the CdSe QD solids passivated by phosphine oxide ligands may have higher mobility of electrons than amine-passivated QD solids. On the other hand, mobility of holes is expected to be higher in QDs capped by amines, since hybridization of MOs in the VB of amine-ligated QDs is higher than in the QDs passivated by phosphine oxide ligands.

3.5. Optical Absorption Spectra. The transition dipole moment between the pair of MOs ψ_k and ψ_l from the VB and the CB is given by $\mu_{kl} = \langle\psi_k|\hat{\mu}|\psi_l\rangle$, $\hat{\mu}$ being the dipole moment operator. To determine the impact of ligands on the optical spectra of the CdSe QD, we decompose μ_{kl} in the single-particle representation into four parts using eq 3 as

$$\mu_{kl} = C_1\mu_{kl}^{QD} + C_2\mu_{kl}^{LG} + C_3\mu_{kl}^{QDLG} + C_4\mu_{kl}^{LGQD} \qquad (4)$$

Here, the first (second) term determines the optical transition of an electron from the occupied state localized on the QD (ligand) to the unoccupied state localized on the QD (ligand). The last two cross-terms correspond to the photoexcited transition of an electron from the VB state localized on the QD to the CB state localized on the ligand and vice versa. The contribution of each part to the total dipole moment is determined by coefficients C_i. Clearly, only hybridized states can contribute to the cross-terms μ_{kl}^{QDLG} and μ_{kl}^{LGQD}, while all states can add to the first two terms.

On the basis of this approach, the absorption spectra of the clusters with different capping agents are calculated, and separate dipolar contributions are compared in Figure 5. The first absorption peak of the isolated single ligand appears around 8 eV (this value is overestimated by 1−1.5 eV compared to

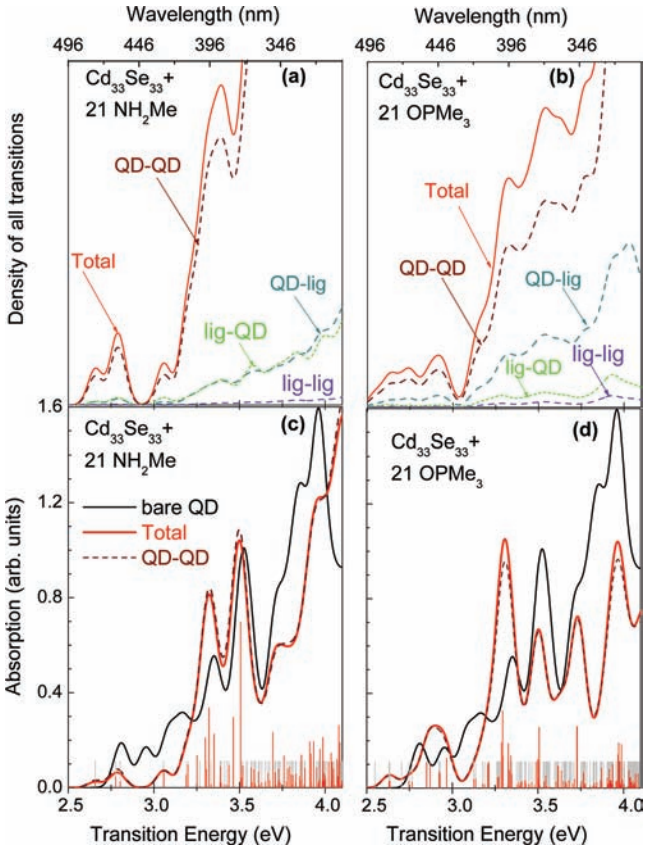

Figure 6. Comparison of the density of transitions spectra and optical spectra of $Cd_{33}Se_{33}$ cluster capped by 21 molecules of NH_2Me (a,c) and $OPMe_3$ (b,d) calculated using line-broadening parameter $\sigma = 30$ meV. The red solid line (a,b) shows the DOS spectra of all possible (including optically forbidden) transitions through the gap. Dashed lines show transitions between valence and conduction bands calculated according to eq 4, decomposing the optical spectrum into four distinct contributions: QD−QD, ligand−ligand, QD−ligand, and ligand−QD. (c,d) The same absorption spectra as shown in Figure 5a,b but in the smaller energy range. Gray vertical lines represent all transitions through the gap, while the red vertical lines correspond to the oscillator strengths of these transitions. Near the energy gap, transitions are dominated by QD transitions and are optically bright. For higher energies, the fraction of transitions between hybridized states increases; however, most of such transitions are dark.

the results of correlated TDDFT calculations, which are important for the analysis of photoexcitations in small molecular species; see Supporting Information, Figure S6). However, in the capped QDs, ligand−ligand transitions occur at much lower energies (5−6 eV), due to the presence of hybridized states closer to the edges of the CB and the VB. On the other hand, the absorption spectrum component coming from the ligand−ligand transitions at energies ~8 eV is significantly higher in amplitude and broader compared to the spectra of the isolated ligands. Observed modifications of the ligand−ligand transitions in the passivated QDs are due to interactions between the neighboring ligands and between ligands and the surface of the cluster. Such interactions induce electron-density polarization, change the transition dipole moments of the ligand states, and result in an overall increase of the oscillator strengths of ligand−ligand transitions. Nevertheless, we observe some additivity in the spectra: the intensities of the spectra arising from ligand−ligand transitions in the cluster capped by 21 and by 9 ligands roughly satisfy the ratio $21/9 = 2.3$, as can be noticed from the comparison of panels b and c in Figure 5.

The polarization effects due to ligand−surface interactions can be clearly seen from comparison of the total spectrum of the capped QD with its partial spectra stemming from QD−QD and ligand−ligand transitions. While the expression for the transition dipole moment of ligated QDs is additive (eq 4), the oscillator strength of the transitions (which is proportional to the square of the transition dipole moment) is not. The total intensity of each spectral term at higher excitation energies is higher than the resulting spectrum of the entire compound. This effect occurs because of the destructive interference between QD−QD, QD−ligand, ligand−QD, and ligand−ligand components: these transition dipole moments are generally oriented in opposite directions, and, consequently, significant cancellations take place. Noteworthy, for the non-interacting QD and ligand case, e.g., when ligands are placed very far from the surface of the QD, the total spectrum of the entire system is completely additive with respect to four components of the transition dipole (not shown). These observations indicate the importance of polarization effects on the spectra due to the ligand−QD interactions. Such behavior of transition dipole components suggests that electronic transitions may have several charge-transfer trends including bulk-to-surface, known as leakage of the electronic wave function outside of the dot[25] and ligand-to-surface. This charge-transfer flow can be seen as a shift of the density distribution in the electron (hole) orbital from the core and ligand regions toward the surface compared to the respective hole (electron) orbitals (see Figure 2).

Figure 5 demonstrates that transitions between the hybridized states (i.e., cross-terms QD−ligand and ligand−QD transitions) become optically allowed for excitation energies larger than $2E_{gap}^{bulk} \sim 4$ eV in all ligated clusters we study. Figure 6c,d displays the same absorption spectra as shown in Figure 5a,b, but in the energy range smaller than $2E_{gap}^{bulk}$. These plots reveal that, at low excitation energies, absorption spectra are solely dominated by QD−QD transitions. However, the profiles of the spectra are different for the bare QD and dots passivated with ligands, demonstrating that the passivating ligands do modify the character of pure QD transitions.

Figure 6a,b shows density of transitions through the band gap in the CdSe cluster capped by 21 molecules of NH_2Me or $OPMe_3$. This figure emphasizes the presence of QD−ligand and ligand−QD transitions that are not seen in the absorption spectra (Figure 6c,d), because most of these transitions are optically inactive. Importantly, the density of the dark QD−ligand and ligand−QD transitions is almost the same in the QDs passivated by amines. This is in a good agreement with the symmetric distribution of the hybridized states at the DOS of this cluster shown in Figure 2c,d. In contrast, there are more dark QD−ligand transitions than ligand−QD transitions in the QD capped by $OPMe_3$. This asymmetry originates from the much higher density of hybrid sates in the CB of the $OPMe_3$-ligated QD than in the VB (Figure 2a,b). Therefore, the transitions from the occupied states localized on the ligand (at least partially) to the unoccupied states localized on the QD are suppressed at small excitation energies; transitions from the QD-localized occupied states to the ligand-localized (or hybridized) unoccupied states dominate. Thus, the surface−ligand interactions lead to the appearance of specific optical transitions in the QD−ligand complex, depending on the ligand type.

The hybridized states near the band gap of the passivated clusters, which do not contribute to the absorption spectra, increase the overall density of electronic states, particularly in the $OPMe_3$-capped cluster (see Figure 6a,b). This near-continuous density of hybridized MOs and possible electron−phonon coupling with the high-frequency vibrations in the ligands could

potentially contribute to phonon-assisted relaxation of high-energy photoexcitations by opening new relaxation channels through these hybridized surface states. Moreover, the difference in the distribution of these states in QDs passivated by amines versus phosphine oxides can be reflected in faster electron relaxation in the QD with TOPO capping compared to amine capping, which was experimentally detected[17] but was not explicitly explained.

4. Conclusions

In summary, we use the $Cd_{33}Se_{33}$ cluster capped by either 9 or 21 molecules of $OPMe_3$ and NH_2Me to computationally model small QDs passivated by commonly used ligands such as TOPO and primary amines. Our DFT calculations reveal significant geometrical reorganization of the surface in both bare and ligated clusters, resulting in the decrease of the average Cd−Se bond lengths on the surface, compared to those inside the QD. The difference in bond lengths on the cluster surface and in the cluster interior contrasts the common idea that QDs are mainly constructed from the bulk-like core atoms and single species of the passivating agents. Yet, the existence and importance of the surface and near-surface layers, which are significantly distinct from the core structure, have been recently evidenced by X-ray photoelectron spectroscopy.[20−22]

Our results reveal that the CdSe QD binds slightly stronger with methylamine than with trimethylphosphine oxide molecules. Both types of passivated ligands typically interact more strongly with two-coordinated Cd atoms on the QD surface than with three-coordinated ones. Because of weak ligand binding to some the three-coordinated Cd atoms, the loss of one such ligand does not significantly affect the electronic and optical spectra of QDs. In contrast, the loss of one of the ligands strongly interacting with two-coordinated Cd atoms leads to the appearance of the trap states inside of the QD band gap. Depending on the geometrical position of the lost ligand (A_1 or C in Figure 1), the trap states might be either optically dark or semi-bright. These results indicate that possible defects in the QD capping, which depend on different experimental procedures of the QD surface treatments, might lead to different optical responses of CdSe QDs.

The calculated density of states and absorption spectra show that pure ligand states are typically situated deep inside the VB of CdSe clusters. However, because of the surface reconstruction and strong bonding between the surface and ligands, we observe substantial charge redistribution and polarization interactions on the surface for fully ligated clusters. Overall these interactions result in the appearance of many hybridized states whose electronic density is delocalized over both QD and the ligand atoms. Such states do not appear inside or at the edges of the band gap of the QD, because surface reorganization suppresses formation of trap states. Typically, optical absorption of hybridized states becomes noticeable in the spectra for excitation energies larger than $2E_{gap}^{bulk} \sim 4$ eV for both capping agents studied. Most of hybridized states that are relatively close to the edges of the CB and the VB are optically dark and are not seen in the absorption spectra. The densities and the positions of the hybridized states with respect to the Fermi level of the system depend on the capping ligands. Hybridized states originating from the methylamine capping contribute equally to the VB and the CB (Figure 2). In contrast, the electronic structure of the CdSe cluster coated with $OPMe_3$ ligands is comprised of very dense hybridized states in the CB, while the presence of such states near the edge of the VB is insignificant (Figure 2).

Hybridized levels in the CB and the VB may enhance the intraband carrier relaxation by opening new relaxation channels: nearly continuous DOS with a dominant character of hybridized MOs and possible electron−phonon coupling with the high-frequency vibrations in the ligands may facilitate intraband carrier relaxation through such surface states. Our results suggest that phosphine oxide ligands, such as commonly used TOPO, might accelerate electron relaxation more efficiently compared to the amine-passivated QDs because of the larger DOS in the CB with a significant contribution from the hybridized states. The efficiency of such a relaxation channel would certainly depend on the electron−phonon interactions and non-adiabatic coupling, which will be verified by future studies. Such phonon-assisted relaxation of high-energy photoexcitations may modify the efficiency of other relaxation mechanisms present such as Coulombic effects, leading, e.g., to the carrier multiplication phenomenon. This allows optimization of desired QDs' functionalities using surface chemistry means.[13]

Acknowledgment. We thank Victor I. Klimov for fruitful discussions and comments, and Arthur Nozik for sending us ref 13 before publication. S.K. is grateful to Oleg V. Prezhdo and Dmitri Kilin for useful suggestions. This work was supported by the DOE Office of Basic Energy Sciences. LANL is operated by Los Alamos National Security, LLC, for the National Nuclear Security Administration of the U.S. Department of Energy under contract DE-AC52-06NA25396. We acknowledge support of Center for Integrated Nanotechnology (CINT) and Center for Nonlinear Studies (CNLS).

Supporting Information Available: Additional details on the calculated electronic structure data of studied QDs; complete refs 33 and 40. This material is available free of charge via the Internet at http://pubs.acs.org.

JA9005749